OUKA
The University of Osaka
Institutional Knowledge Archive

Title	Effects of flow rate on sensitivity and affinity in flow injection biosensor systems studied by 55-MHz wireless quartz crystal microbalance
Author(s)	Ogi, Hirotsugu; Fukunishi, Yuji; Omori, Toshinobu et al.
Citation	Analytical Chemistry. 2008, 80(14), p. 5494-5500
Version Type	AM
URL	https://hdl.handle.net/11094/84138
rights	This document is the Accepted Manuscript version of a Published Work that appeared in final form in Analytical Chemistry, © American Chemical Society after peer review and technical editing by the publisher. To access the final edited and published work see https://doi.org/10.1021/ac800459g.
Note	

The University of Osaka Institutional Knowledge Archive : OUKA

https://ir.library.osaka-u.ac.jp/

The University of Osaka

Effects of Flow Rate on Sensitivity and Affinity in Flow-Injection Biosensor Systems Studied by 55-MHz Wireless QCM

Journal:	*Analytical Chemistry*
Manuscript ID:	draft
Manuscript Type:	Article
Date Submitted by the Author:	n/a
Complete List of Authors:	Ogi, Hirotsugu; Osaka University, Graduate School of Engineering Science Fukunishi, Yuji; Osaka University, Graduate School of Engineering Science Omori, Toshinobu; Osaka University, Graduate School of Engineering Science Hatanaka, Kenichi; Osaka University Hirao, Masahiko; Osaka University, Graduate School of Engineering Science Nishiyama, Masayoshi; Osaka University, Renovation Center of Instruments for Science Education and Technology

Effects of Flow Rate on Sensitivity and Affinity in Flow-Injection Biosensor Systems Studied by 55-MHz Wireless QCM

Hirotsugu Ogi, Yuji Fukunishi, Toshinobu Omori, Kenichi Hatanaka, Masahiko Hirao, and Masayoshi Nishiyama[*]

Graduate School of Engineering Science, Osaka University. Toyonaka, Osaka 560-8531, Japan

[*]Renovation Center of Instruments for Science Education and Technology, Osaka University Machikaneyama 1-2, Toyonaka, Osaka 560-8531, Japan

RECEIVED DATE

TITLE RUNNING HEAD: 55 MHz Wireless QCM and Flow Effect on Affinity

CORRESPONDING AUTHOR FOOTNOTE

Hirotsugu Ogi, Tel. +81-6+6850-6187, Fax: +81-6-6850-6187, E-mail: ogi@me.es.osaka-u.ac.jp

ABSTRACT

In this paper, we develop a 55-MHz wireless-electrodeless quartz-crystal microbalance (QCM) and systematically study effects of the flow rate on the sensitivity to the detection of proteins and on the affinity between biomolecules evaluated by the flow-injection system. Brownian motion of proteins in liquid suggests low probability of meeting, and the convection effect plays an important role in the sensitivity and the affinity in the flow-cell-injection system. The wireless quartz crystal is isolated in the QCM cell and the flow rates between 50 and 1,000 μl/min were used for monitoring binding reactions between human immunoglobulin G and staphylococcus-aureus protein A. The sensitivity is significantly increased as the flow rate increased, while the affinity value remained unchanged. However, the affinity value has been affected by the reaction time for a large concentration analyte, indicating the need of a high-sensitive biosensor system for accurate evaluation of affinity. The electrode effect on the QCM sensitivity is also quantitatively investigated, showing that the electrode significantly deteriorates the QCM sensitivity and makes the Sauerbrey equation invalid.

KEYWORDS Biosensors, Flow rate, Affinity, Sensitivity, Quartz crystal microbalance, Wireless

The importance of the affinity measurement among various biomolecules has been recognized during the progress in protein design and development of drugs. Various tag proteins have been reported for affinity evaluation and purification to product recombinant proteins. However, conventional affinity tag systems use large-size tag proteins such as green-fluorescent proteins (GFPs) (~>27 kDa), FLAGs with specific antibodies (~>150 kDa), and quantum dots (>~20 Å)[1, 2] and have influence on the apparent affinity among biomolecules. Furthermore, individual affinity tags require their specific buffer conditions, which will affect functions of examined proteins.[3] Therefore, significant efforts have been paid for developing small-size tags, which do not affect functions of proteins of interest.[4, 5]

The label-free methods are then important for studying inherent interactions of biomolecules. Two methods are widely recognized. One is the surface-plasmon-resonance (SPR) biosensor.[6-8] A conventional SPR measurement monitors interactions between a receptor protein and an analyte injected in a flow-injection system. The receptor is immobilized on a metallic thin film deposited on a glass plate, which is irradiated from the back surface through a prism by a light. The coupling condition (the resonance condition) between the evanescent field generated by the incident light and the propagating surface plasmon wave (SPW) at the metallic film is affected by the macroscopic electric properties in the evanescent field, and the incident angle of the light for SPR changes during the binding reaction between proteins. Monitoring the incident angle as the biding reaction progresses enables evaluation of kinetics of reactions between the molecules. The other is the quartz-crystal-microbalance (QCM) biosensor.[9-15] It allows determination of the mass of adsorbed proteins on the receptor immobilized on a quartz oscillator through the decrease of the resonance frequency,[16,17] realizing a real-time monitoring of association and dissociation reactions between molecules. Because the fractional-frequency change equals the ratio of the adsorbed mass to the oscillator mass, the QCM biosensor allows quantitative measurement for the biding rate and affinity without calibrations. The most important advantage of the

QCM biosensor is the quantitative nature, while the SPR measurement involves ambiguity regarding the relationship between the incident angle and the amount of the adsorbed proteins.

These label-free biosensors have to measure quite small changes in physical quantities caused by biomolecules. Changes in resonance frequency observed in conventional QCMs are typically smaller than 0.001%, for example. Flow-injection systems have been then adopted: A surface-modified sensor is set in a flow cannel and a carrier solution steadily flows through the sensor surface. When the physical response becomes stable enough, the analyte is injected. The relative change in the physical property is then detected to evaluate kinetics of the reaction. Because of the relative change from the steady condition, high-sensitive detection of the analyte is possible. However, in the evaluation of affinity, we have to concern on the effect of the flow rate, because the convection will play an important role in the reaction rather than the self diffusion of molecules. The important advantage of the flow-injection system is that it allows us to assume constant concentration of the analyte during reaction, making the thermodynamic analysis easy and accurate. The analyte concentration, however, decreases and increases at the local sensor-surface region in the case of association and dissociation reactions, respectively. Brownian motion is not dominant compared with the reaction time, and the convection makes the concentration of the surrounding solution recover. Thus, the sensitivity and apparent affinity may be dependent on the flow rate and it is important to investigate this effect quantitatively.

There are three purposes in this study. First, we establish a 55-MHz wireless-electrodess QCM. Previously, we suggested significant influence of electrodes on quartz surfaces on the QCM sensitivity and proposed a noncontacting measurement of the resonance frequency for electrodess quartz plates by the line antenna.[11, 12, 18] The affinity has to be evaluated using lower-concentration solutions to avoid steric hindrance among biomolecules as shown later, and a high-sensitive QCM is required. Because the QCM sensitivity increases as the thickness of the oscillator decreases, we here develop the noncontacting method for the 30-μm-thick AT-cut quartz and achieve a 55-MHz wireless QCM. Using the specific binding between human immunoglobulin G (IgG) and staphylococcus aureus protein A (SpA), we demonstrate high sensitivity and usefulness of the QCM developed here. Second, we

investigate the effect of the electrode on the QCM sensitivity by solving five-layered oscillator model. The electrode causes two critical problems; it deteriorates the QCM sensitivity, and it limits the use of the Sauerbrey equation. QCM results have been analyzed on the basis of the Sauerbrey equation, which, however, does not apply to thinner oscillators with gold electrodes. Thus, we have to discuss the applicability of the Sauerbrey equation. Third, we investigate the effect of the flow rate in the range between 50 and 1,000 μl/min on the sensitivity and affinity using the QCM-flow-injection system. These results indicate that the flow rate highly affects the sensitivity but does not affect the apparent affinity.

VIBRATIONAL ANALYSIS OF MULTILAYERED QCM

The Sauerbrey equation[16] estimates the frequency change Δf caused by adsorption of a mass Δm on the oscillator surface by $\Delta f = -f\Delta m/M_q$, where M_q denotes the mass of the quartz crystal. Thus, there is a linear relationship between the adsorbed mass and the frequency change, which has been used for quantitative analysis of QCM results. Modification of the Sauerbrey equation gives

$$\Delta f = -\frac{\rho_s v_q}{2\rho_q} \cdot \frac{1}{d_q^2} . \quad (1)$$

Here, v_q, ρ_q, and d_q are the shear-wave velocity, the mass density, and the thickness of the quartz crystal, respectively. ρ_s denotes the area mass density of the adsorbed substance. Therefore, the QCM sensitivity $|\Delta f|$ is inversely proportional to the square of the thickness of the oscillator, and it is obvious that thinner oscillator provides higher sensitivity. Equation (1) shows good agreement with measurements when the oscillator is thick enough compared with the electrodeless thickness. However, thinning the oscillator increases the inertia resistance of the electrode layers and causes elastic coupling of the acoustic wave with protein layers,[11] leading to discrepancy from the Sauerbrey equation.[12] Especially, Au films were usually used as electrodes because of their high association with thiol compounds, but the mass density of Au is considerably larger than that of α-quartz by a factor 7.3,

causing very high inertia resistance at the oscillator surfaces, where the vibrational acceleration takes the maximum.

We then have to investigate the limitation of the Sauerbrey equation in the use of a thinner QCM. When both surfaces are used as the QCM sensor, the oscillator consists of five layers; middle α-quartz layer, two electrodes layers sandwiching it, and two protein layers adsorbed on the electrodes. However, our previous calculations assumed three layers for the one-side use for simplicity. We here propose more generalized vibrational analysis for plane-shear-wave resonances in a multilayer system consisting of *n* layers as shown in Fig. 1. The partial waves in individual layers are expressed by

$$u_i^{(\pm)} = A_i^{(\mp)} e^{\mp \mathrm{j} k_i z}, \tag{2}$$

where, u_i and A_i denote the horizontal displacement and the complex amplitude in the *i*th layer, respectively. (The term $e^{j\omega t}$ is omitted.) $\mathrm{j} = \sqrt{-1}$. The superscripts (+) and (-) denote quantities for downward and upward partial plane waves, respectively. k_i is the wavenumber at the *i*th layer given by

$$k_i = 2\pi f \sqrt{\frac{G_i}{\rho_i}}. \tag{3}$$

Here, G_i and ρ_i are the shear modulus and the mass density at the *i*th layer, respectively. The boundary conditions for continuity of the displacement and the shear stress are as follows:

$$G_1\left(\frac{\partial u_1^{(+)}}{\partial z} + \frac{\partial u_1^{(-)}}{\partial z}\right) = 0 \quad \text{at } z=0, \tag{4}$$

$$G_n\left(\frac{\partial u_n^{(+)}}{\partial z} + \frac{\partial u_n^{(-)}}{\partial z}\right) = 0 \quad \text{at } z=D_n, \tag{5}$$

$$u_i^{(+)} + u_i^{(-)} = u_{i+1}^{(+)} + u_{i+1}^{(-)} \quad \text{at } z=D_i, \text{ and} \tag{6}$$

$$G_i\left(\frac{\partial u_i^{(+)}}{\partial z} + \frac{\partial u_i^{(-)}}{\partial z}\right) = G_{i+1}\left(\frac{\partial u_{i+1}^{(+)}}{\partial z} + \frac{\partial u_{i+1}^{(-)}}{\partial z}\right) \quad \text{at } z=D_i. \tag{7}$$

Here, D_i is the distance of the ith interface from the top surface (Fig. 1). Substitution of Eq. (2) into Eqs. (4)-(7) falls into an eigenvalue problem $\Gamma\mathbf{A}=0$ with a matrix Γ of $(2n)\times(2n)$. The vector $\mathbf{A} = (A_1^{(+)}, A_2^{(+)}, \cdots, A_n^{(+)}, A_1^{(-)}, A_2^{(-)}, \cdots, A_n^{(-)})^{\mathrm{T}}$ consists of the complex amplitudes. Thus, resonance frequencies of the multilayer are obtained from eigenvalues of Γ by solving $\det[\Gamma]=0$, from which we exactly calculated the resonance frequency for actual QCM oscillators.

EXPERIMENTAL SECTION

Surface preparation. A 30-μm-thick AT-cut quartz plate with 5×4 mm^2 was used, whose fundamental resonance frequency was near 55 MHz. It was cleaned in a piranha solution (98%H_2SO_4:33%H_2O_2=7:3), and 18-nm Au thin films were deposited after 2-nm Cr thin films on both surfaces by the magnetron spattering method for the subsequent gold-alkanethiol binding reaction. (The 20-nm-thin films hardly affect the sensitivity and the availability of the Sauerbrey equation, as shown later.) It was cleaned again in the piranha solution, rinsed with ultrapure water several times, and immersed in a 10 mM 10-carboxy-1-decanethiol/absolute ethanol solution for 20 h at 4 °C. After rinsing with absolute ethanol three times, the oscillator was set in the handmade sensor cell[11, 12] by softly sandwiching a part of the edge by silicon rubber sheets. The QCM cell was then installed in the homebuilt flow-injection system as shown in Fig. 2, and the immobilization of SpA was performed in the flow-injection system as follows. The resonance frequency was monitored in a noncontacting manner as will be shown later until the fractional-frequency variation was smaller than 10^{-6}, while the phosphate-buffer solution (PBS; pH 7.4) flowed at the flow rate of 200 μl/min as a carrier buffer. Then, the solutions of 100 mM EDC (1-ethyl-3-(3-dimethylaminopropyl)carbodiimide, hydrochloride) and 0.4 mg/ml SpA/PBS were injected for 1 h to activate the carboxyl terminals and immobilize SpA molecules. A 10 mg/ml bovine-serum-albumin (BSA) solution was then injected for blocking the remaining activated sites to avoid a nonspecific binding of IgG, which was followed by injections of analyte solutions.

Human IgG was from Athens Research and Technology, Inc. (product num. 16-16-090707; purity ~95%). SpA was from Zymed Laboratories, Inc. (product num. 10-1100; purity 98%). 10-carboxy-1-decanethiol (product num. C385) and EDC (product num. W001) were from Dojindo Laboratories. BSA (No. 9048-46-8) were from Sigma-Aldrich Japan. All of other chemical substances were purchased from Wako Pure Chemical Industries Ltd.

Experimental procedure. The micropump provided a steady flow of the PBS carrier solution. The switching valve selected one analyte solution to be injected among eight vials, which flowed into the sensor cell through the degasifier. The 3-m Teflon tube column made the solution temperature stable at a set value (37 °C). Tone bursts were applied to the generation antenna to generate shear-horizontal vibration of the quartz in a noncontacting manner.[19] After the excitation, the detection antenna received reverberation signals, which entered into the superheterodyne spectrometer to measure the phase and amplitude of the received signals using the driving signal as the reference.[20] Frequency scanning determines resonance frequency from peak-amplitude frequency, which was repeated until resonance frequency became sufficiently stable. We then monitored the phase of the signal to make a quick measurement (~0.1 s). The frequency change was determined from the linear relationship between frequency and phase around a resonance.[12]

The IgG solutions were injected after the blocking procedure. The typical injection sequence was as follows. (i) Injection of an IgG solution, (ii) injection of PBS, (iii) injection of glycine-HCl buffer (GHB) (0.1 M, pH 2.4) for dissolve the IgG-SpA binding, (iv) injection of PBS, and (v) injection of next IgG solution (returning to (i)). The concentration of IgG and the flow rate were changed for investigating the sensitivity, the affinity, and the effects of the flow rate on them.

RESULTS AND DISCUSSION

Electrode Effect. Figure 3(a) shows the frequency change calculated for adsorption of 1-nm protein layers on both surfaces. We assumed the shear modulus and the mass density of outer protein layers to be 0.1 GPa and 1,500 kg/m^3, respectively, and we used G_q=29 GPa and ρ_q=2650 kg/m^3 for AT-cut quartz,[21] and G_{Au}=28 GPa and ρ_{Au}=19,284 kg/m^3 for Au layers. Broken lines in Fig. 3(a) are the estimation with the Sauerbrey equation (Eq. (1)). For a conventional QCM sensor with a 200-μm-thick quartz plate, deposited electrodes affect little the sensitivity, and the difference of the actual frequency change from the Sauerbrey prediction is marginal. However, when the quartz thickness becomes smaller, the sensitivity increases, but the presence of electrode layers deteriorates the sensitivity. For example, 500-nm-thick electrodes on surfaces of a 30-μm-thick-quartz plate decrease the amount of the frequency change by 40%. Thus, the electrodes significantly deteriorate the QCM sensitivity when the oscillator becomes thinner. Furthermore, the Sauerbrey equation cannot be applied for thicker electrodes, lowering the reliability of the thermodynamic analysis for affinity. Figure 3(b) shows the change of the resonance frequency caused by the adsorption of the protein. The sensitivity of the 30-μm-thick QCM is lowered only by the electrodes. Thus, the electrodeless approach is an important key for achieving high-sensitive and quantitative QCM biosensors. In the present study, we used 20-nm-thick Au/Cr films; their effects on the sensitivity and the Sauerbrey equation can be neglected from the results of Figs. 3(a) and (b).

Repeatability of the sensor. We used one sensor tip for many measurements of the interaction between IgG and SpA, and the repeatability was confirmed in advance. Figure 4 shows the typical as-measured frequency response for an injection sequence. The resonance frequency decreased exponentially when the IgG solution reached the QCM cell. After the injection of the GHB solution, the resonance frequency increased beyond the baseline, but it recovered by the injection of PBS. The sensor tip then

showed nearly identical performance. Figures 5(a) and (b) show binding curves observed for IgG solutions of different concentrations between 67 pM and 67 nM. The binding reaction is clearly observed even for a low-concentration solution after several dissociation procedures. The repeatability was well confirmed for 20 injections for a single sensor tip. We used a sensor tip for ~10 measurements, and replaced it with a new tip.

Kinetic Analysis. Resonance-frequency change can be incorporated in the chemical-kinetics theory when three assumptions are satisfied. First, the reaction occurs with a pseudo-first-order manner. Second, the concentration of the injected IgG solution remains unchanged throughout the reaction. Third, the Sauerbrey equation is satisfied; that is, the amount of the frequency shift is proportional to the amount of the adsorbed IgG molecules on protein A. Based on these assumptions, the relationship between the frequency change and the kinetics of the binding reaction has been formulated as[10, 17]

$$\Delta f(t) = \Delta f_e\left(\mathrm{e}^{-\alpha t} - 1\right), \tag{8}$$

$$\alpha = k_a C_{\mathrm{IgG}} + k_d . \tag{9}$$

Here, Δf_e is the frequency change at the equilibrium state. C_{IgG} is the concentration of IgG. k_a and k_d are association-rate and dissociation-rate constants, respectively. The equilibrium constant K_A given by

$$K_A = \frac{k_a}{k_d}, \tag{10}$$

indicates the affinity between the two molecules. Equations (8) and (9) show that the frequency change obeys the exponential function and the exponential coefficient is proportional to C_{IgG}. Therefore, plotting α versus C_{IgG} provides a line, whose slope and intercept provide k_a and k_d, respectively, yielding K_A.

Hindrance Effect and Kinetic Constants. Figure 6 shows binding curves for injections of IgG solutions of various concentrations. Solid lines are the fitted theoretical function (Eq. (8)). When the IgG solution arrives at the sensor cell, the frequency starts to decrease exponentially, and the theoretical function in Eq. (8) completely fits to the frequency change for lower-concentration solutions. Thus, the three assumptions made above are essentially validated. However, for higher-concentration solutions (C_{IgG}>34 nM), a single exponential function fails to fit to the observed frequency change, and two exponential functions are apparently required to explain the frequency change. The critical value, at which the frequency change departs form the first exponential function, appears around $\Delta f/f$=-9.5×10^{-5} (Δf=-5.2 kHz).

This critical value can be consistently explained from the steric-hindrance effect of IgG molecules: The Sauerbrey equation converts the critical value into the adsorbed mass of the IgG molecules on the quartz surfaces of 1.5×10^{-7} g, corresponding to the total number of molecules of 6.1×10^{11}. The effective area of the QCM sensor is 5×4×2 mm^2, which yields the occupation area of a single molecule (66 nm^2), and the diameter of the equivalent sphere of 9.2 nm. On the other hand, the volume of a single IgG molecule is about 14.2×3.8×4.5 nm^3,[22] corresponding to the equivalent sphere with a diameter of 7.7 nm. These two representative diameters are in good agreement. Therefore, at the critical point, almost the whole surfaces of the oscillator were covered by IgG molecules, and the steric hindrance subsequently occurred, resulting in deceleration of binding affinity because of buried binding sites.

This result gives an important indication in the determination of kinetic constants using a flow-injection system. Previous QCMs used only one sides of their oscillators, and when the conventional 9-MHz QCM is used, for example, the critical value will be $\Delta f/f$=-0.78×10^{-5} or Δf=-70 Hz. Therefore, the affinity evaluation must be performed using small frequency change; otherwise, the affinity value is underestimated. Furthermore, not only QCMs but also SPR immunoassays adopted flow-injection

systems to evaluate kinetics of biomolecule reactions, and they have to use low concentration analyte solutions or physical responses before the steric-hindrance effects becomes dominant.

We thus determined the affinity value using the data below the critical frequency change. Figure 7 shows the relationship between α and C_{IgG}. The solid line represents the theory, giving k_a, k_d, and K_A.

Effects of Flow Rate. Increasing the flow rate considerably accelerated the binding reaction as shown in Fig. 8. We investigated the effect of the flow rate on the kinetic constants between 50 and 1,000 μl/min, corresponding to flow velocities between 0.11 and 2.22 mm/s in the sensor cell, respectively. Figure 9 shows the result. Both association and dissociation kinetic constants, k_a and k_d, increase as the flow rate increases.

We attribute this observation to the variation of the local concentration of the analyte. As the binding reaction progresses, the concentration of the analyte locally decreases near the interaction surface, and it should recover in a time shorter enough than the reaction time; otherwise, the apparent association constant decreases because the analyte concentration is assumed to be unchanged. Similarly, the local concentration of the analyte near the surface is increased in the progress of the dissociation reaction in a later stage, leading to the decrease of the apparent dissociation constant. Therefore, the concentration variation of the surrounding solution should be minimized. Self diffusion of biomolecules in liquids is, however, insufficient to make the concentration stable because of their larger molecular masses. To confirm this, we calculate the time needed for a molecule to move to the mean-free path. According to the Einstein equation for Brownian motion,[23] the average distance σ for a molecule to move in time t due to Brownian motion is given by $\sigma = \sqrt{2Dt}$. D denotes the diffusion coefficient and is reported to be 7.4×10^{-11} m^2/s for an IgG molecule in liquid.[24] Thus, the time needed to move to the mean-free path is calculated when the analyte concentration is known. (We estimated the mean-free path as the average distance between molecules.) This time is compared with that caused by the flow of

the analyte in Fig. 10. The time to carry an IgG molecule to the mean-free path by the flow decreases as the flow rate increases, and it is largely shorter than that caused by Brownian motion. For the analyte concentration of 0.67 nM, for example, the flow significantly contributes to keep the concentration unchanged. Thus, larger flow rate is required for increasing the sensitivity and making the kinetic analysis appropriate. More important observation is that the equilibrium constant K_A is nearly independent of the flow rate (Fig. 9), because the flow effect is canceled by taking a ratio between k_a and k_d. This conveniently justifies affinity values determined by QCM and SPR methods in the past, although the association and dissociation constants would include serious errors.

CONCLUSION

A 55-MHz wireless-electrodeless QCM system was homebuilt and the fundamental resonance frequency was measured by the line antenna contactlessly. It showed high sensitivity in the detection of IgG solution by SpA immobilized on both surfaces of the 30-μm-thick oscillator. The binding curve was obtained for IgG solutions of concentrations between 67 pM and 134 nM, showing high repeatability. The measured frequency change was well explained by the chemical-kinetic theory.

The electrode effect was investigated for five layered oscillators which demonstrated significant influence of the Au electrodes on the sensitivity and the availability of the Sauerbrey equation. 500-nm-thick Au films on both surfaces decrease the sensitivity by 40%.

The steric hindrance effect was quantitatively discussed. The critical frequency values were -5.2 kHz for the 30-μm-thick (55-MHz) oscillator and -70 Hz for a conventional 9-MHz oscillator, respectively. Under these values, the apparent affinity value is decreased.

The flow rate effect on the kinetic constants were systematically studied. The association-rate and dissociation-rate constants are significantly increased by the increase of the flow rate. Brownian motion is insufficient to keep the concentration of the surrounding analyte constant. However, the equilibrium

constant K_A remains unchanged, indicating that previously reported affinity values using QCMs and SPRs with the flow-injection system are valid.

Acknowledgement

A part of this study was supported by Life Phenomena and Measurement Analysis, PRESTO, by Japan Science and Technology Agency.

1. Green, M. *Angew. Chem. Int. Ed.* 2004, **43**, 4129-4131.
2. Bruchez, M.; Moronne, M.; Gin, P.; Weiss, S.; Alivisatos, A. *Science* 1998, **281**, 2013-2016.
3. Terpe, K. *Appl. Microbiol. Biotechnol.* 2003, **60**, 523-533.
4. Guignet, E.; Hovius, R.; Vogel H. *Nat. Biotechnol.* 2004, **22**, 440-444.
5. Ojida, A.; Honda, K.; Shinmi, D.; Kiyonaka, S.; Mori, Y.; Hamachi I. *J. Am. Chem. Soc.* 2006, **128**, 10452-10459.
6. Kurita, R.; Yokota, Y.; Ueda, A.; Niwa, O. *Anal. Chem.* 2007, **79**, 9572-9576.
7. Nedelkov, D. *Anal. Chem.* 2007, **79**, 5987-5990.
8. Hoaa, X.; Kirk, A.; Tabrizian, M. Biosens. Bioelectron. 2007, **23**, 151–160.
9. Muramatsu, H.; Dicks, M.; Tamiya, E.; Karube, I. *Anal. Chem.* 1987, **59**, 2760-2763.
10. Liu, Y.; Yu, X.; Zhao, R.; Shangguan, D.; Bo, Z.; Liu. G. *Biosens. Bioelectron.* 2003, **19**, 9-19.
11. Ogi, H.; Motohisa, K.; Matsumoto, T.; Hatanaka, K.; Hirao, M. *Anal. Chem.* 2006, **78**, 6903-6909.
12. Ogi, H.; Motohisa, K.; Hatanaka, K.; Ohmori, T.; Hirao, M.; Nishiyama, M. *Biosens. Bioelectron.* 2007, **22**, 3238–3242.
13. Pei, Y.; Yu, H.; Pei, Z.; Theurer, M.; Ammer, C.; Andre, S.; Gabius, H.-J.; Yan, M.; Ramstrom, O. *Anal. Chem.* 2007, **79,** 6897-6902.
14. Shen, Z.; Huang, M.; Xiao, C.; Zhang, Y.; Zeng, X.; Wang, P. G. *Anal. Chem.* 2007, **79**, 2312-2319.
15. Furusawa, H.; Takano, H.; Okahata, Y. *Anal. Chem.* 2008, **80**, 1005-1011.
16. Sauerbrey, G. *Z. Phys.* 1959, **155**, 206-222.

17. Eddowes, M. J. Biosensors 1987, **3**, 1-15.

18. Ogi, H.; Motohisa, K.; Hatanaka, K.; Ohmori, T.; Hirao, M.; Nishiyama, M. Jpn. J. Appl. Phys. 2007, **46**, 4693-4697.

19. Ogi, H.; Niho, H.; Hirao, M. *Appl. Phys. Lett.* 2006, **88**, 141110.

20. Hirao, M.; Ogi, H. *EMATs for Science and Industry: Noncontacting Ultrasonic Measurements*. (Springer/Kluwer, Boston, 2003).

21. Ogi, H.; Ohmori, T.; Nakamura, N.; Hirao, M. *J. Appl. Phys.* 2006, **100**, 053511.

22. Sarma, V.; Silverton, E.; Davies, D; Terry, W. *J. Biol. Chem.* 1971, **246**, 3753-3759.

23. Einstein, A. Annal. Phys. 1905, **17**, 549-560.

24. Karlsson, D.; Zacchi, G.; Axelsson, A. *Biotechnol. Prog.* 2002, **18**, 1423-1430.

FIGURE CAPTIONS

Figure 1. Partial plane waves propagating in a multilayered oscillator.

Figure 2. Homebuilt wireless-electrodeless QCM system.

Figure 3. (a) Amount of the frequency change caused by the adsorption of 1-nm protein layers on both surfaces on Au electrodes. Solid curves are the exact solutions for five-layered oscillators and broken lines are the predictions from the Sauerbrey equation. (b) Amount of the frequency change caused by the increase of the thickness of the protein layers for a 30-μm-thick oscillator with various electrode thickness.

Figure 4. As-measured frequency response for an injection sequence. Arrows indicate the arrival time of solutions at the sensor cell. SpA, BSA, GHB, PBS, and IgG mean staphylococcus-aureus, bovine-serum-albumin, glycin-HCl-buffer, and phosphate-buffer solutions, respectively.

Figure 5. (a) As-measured frequency response and (b) binding curves for injections of IgG solutions of various concentrations between 67 pM and 67 nM. Note that a logarithmic scale is used in (b).

Figure 6. Binding curves for injections of IgG solutions of various concentrations. The solid curves are fitted theory (Eq. (8)). The horizontal broken line indicates the critical value, blow which the steric-hindrance effect becomes significant and decreases the affinity.

Figure 7. Langmuir plot for the concentration of IgG (C_{IgG}) versus the exponential coefficient (α) to determine the kinetic constants. The solid line denotes the fitted theoretical function (Eq. (9)). Note that a logarithmic scale is used for the horizontal axis. The flow rate was 500 μl/min.

Figure 8. Frequency responses for injection of 6.7-nM IgG solution at various flow rates. The logarithmic scale is used. The solid lines are fitted theoretical functions (Eq. (8)), showing good agreement with measurements. The numbers denote the flow rate in μl/min.

Figure 9. Correlations of the association-rate constant k_a, the dissociation-rate constant k_d, and the equilibrium constant K_A with the flow rate.

Figure 10. Relationship between the flow rate and the time for an IgG molecule to move to the mean-free path. BM denotes the movement by Brownian motion.

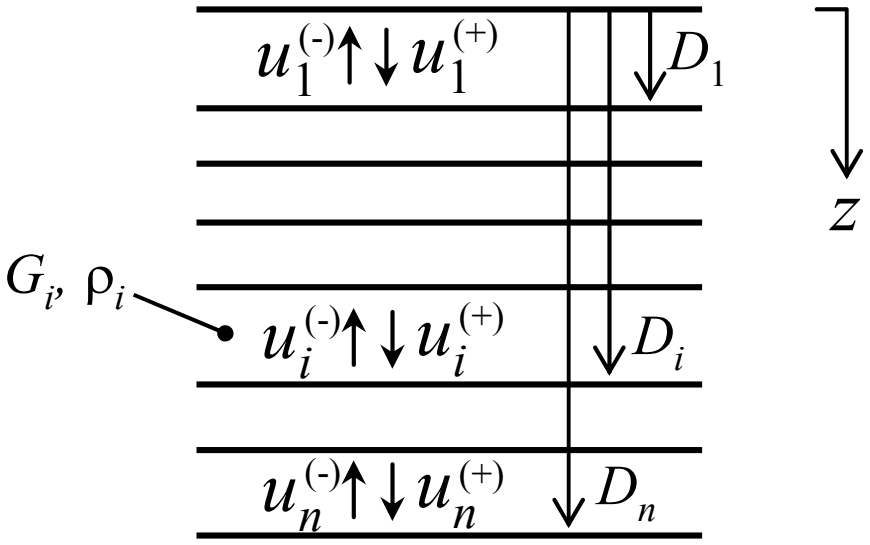
$u_1^{(-)} \uparrow\downarrow u_1^{(+)}$
D_1
z
$G_i,\ \rho_i$
$u_i^{(-)} \uparrow\downarrow u_i^{(+)}$
D_i
$u_n^{(-)} \uparrow\downarrow u_n^{(+)}$
D_n

Fig. 1

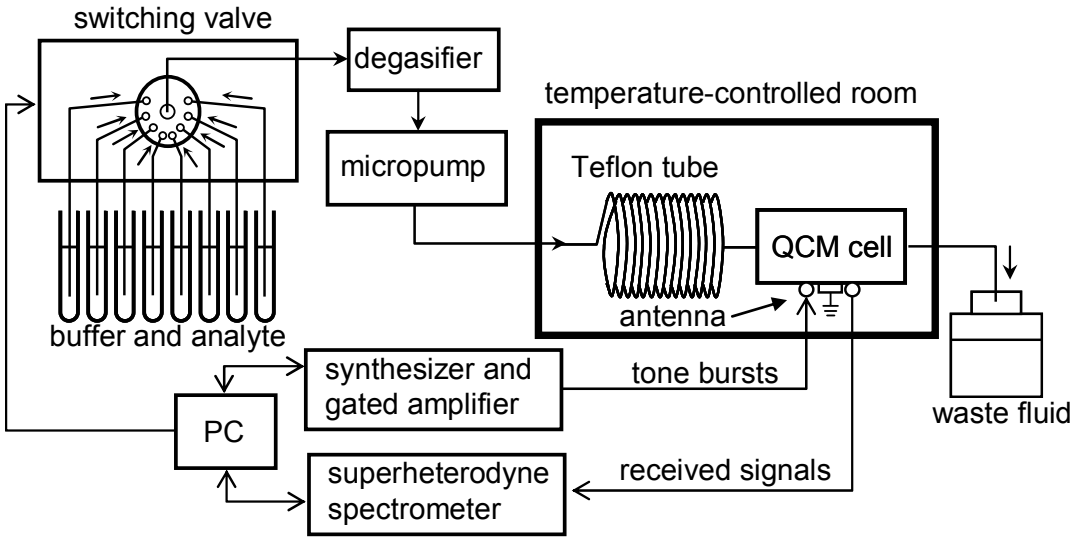
switching valve
degasifier
temperature-controlled room
micropump
Teflon tube
QCM cell
antenna
buffer and analyte
synthesizer and
gated amplifier
tone bursts
waste fluid
PC
superheterodyne
spectrometer
received signals

Fig. 2

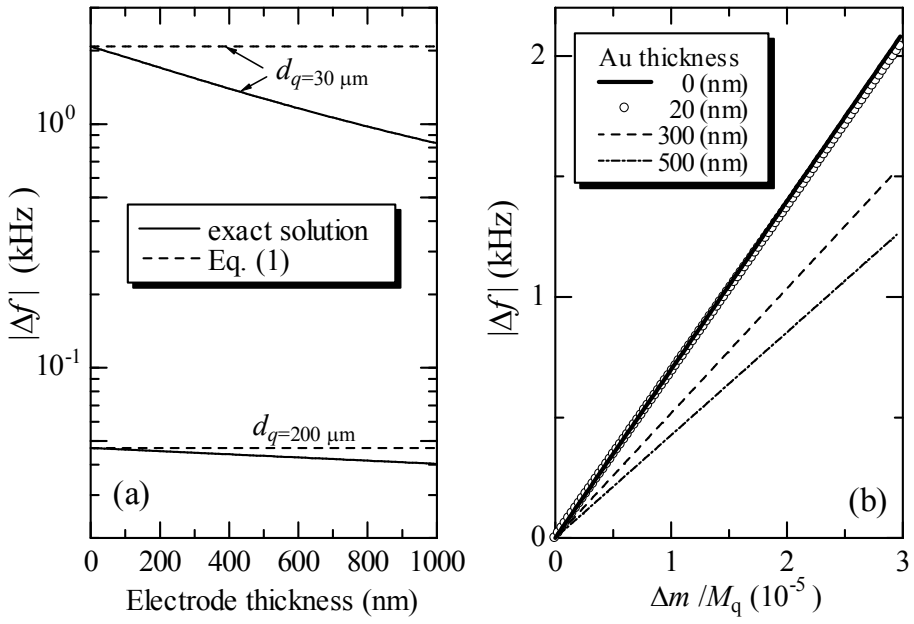
d_q=30 μm
10^0
10^{-1}
exact solution
Eq. (1)
d_q=200 μm
(a)
|Δf| (kHz)
0 200 400 600 800 1000
Electrode thickness (nm)
Au thickness
0 (nm)
20 (nm)
300 (nm)
500 (nm)
(b)
|Δf| (kHz)
0 1 2
0 1 2 3
Δm /M_q (10^{-5})

Fig. 3

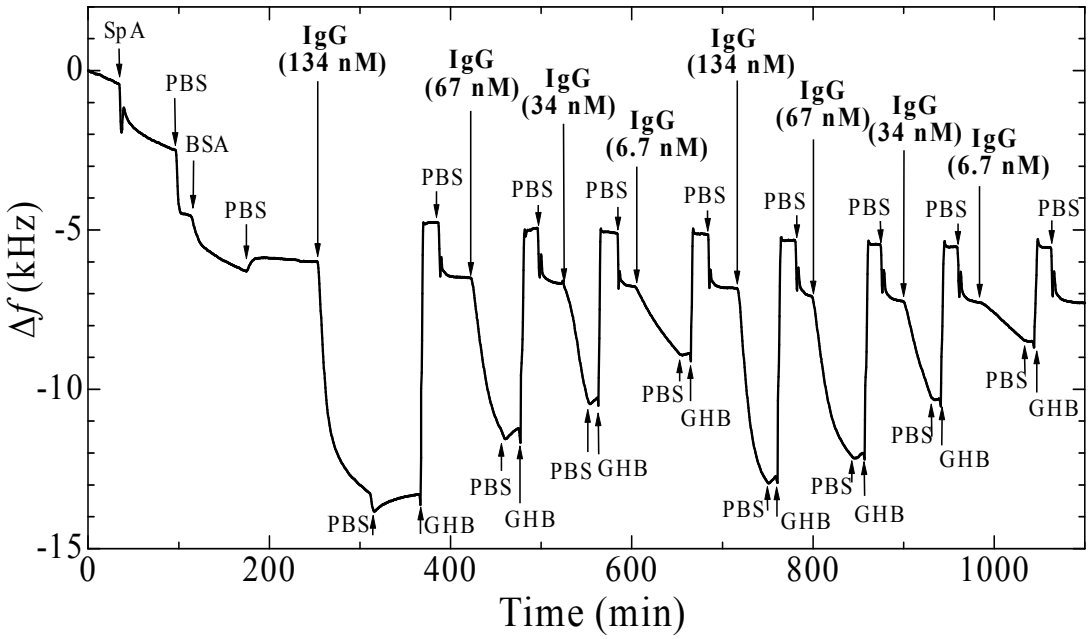
SpA
PBS
BSA
PBS
IgG (134 nM)
PBS
GHB
IgG (67 nM)
PBS
GHB
IgG (34 nM)
PBS
GHB
IgG (6.7 nM)
PBS
GHB
IgG (134 nM)
PBS
GHB
IgG (67 nM)
PBS
GHB
IgG (34 nM)
PBS
GHB
IgG (6.7 nM)
PBS
GHB
PBS
Δf (kHz)
0
-5
-10
-15
0
200
400
600
800
1000
Time (min)

Fig. 4

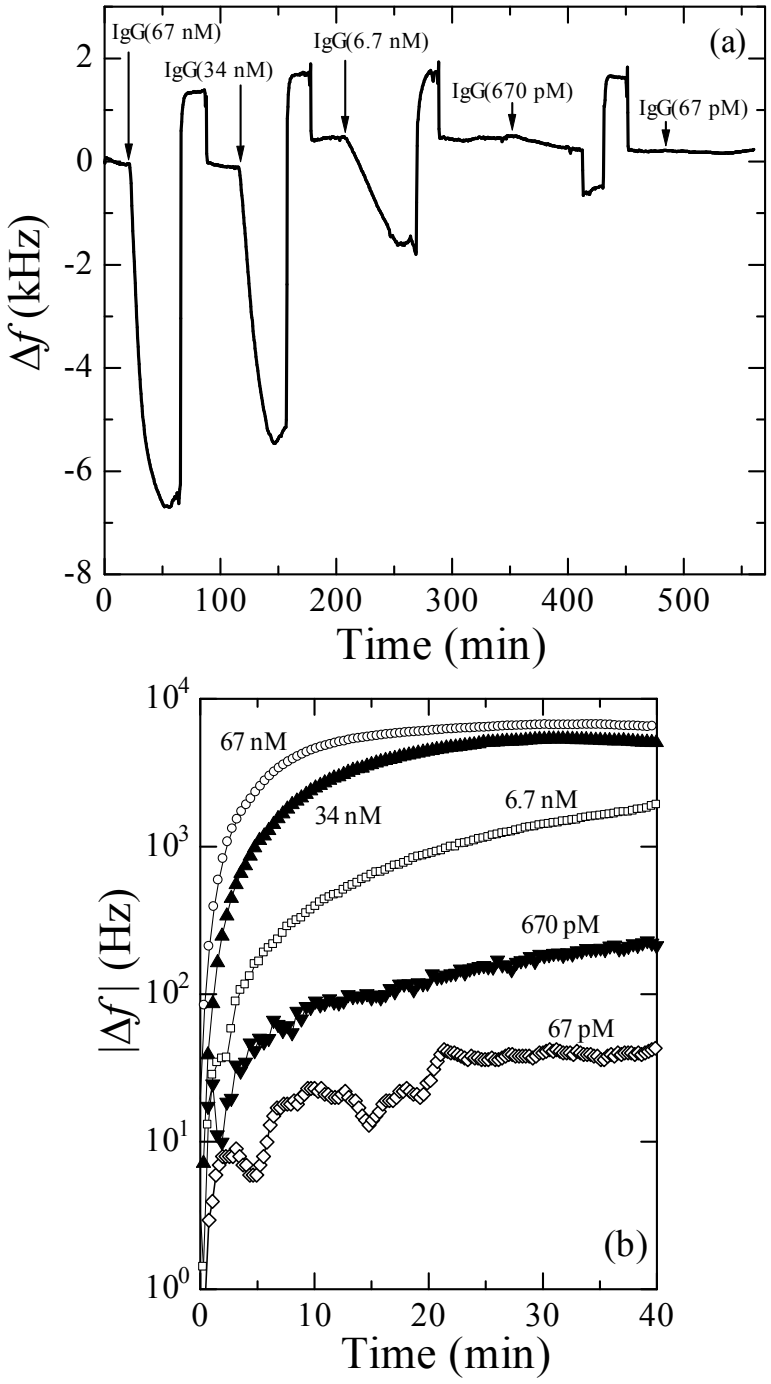
IgG(67 nM)
IgG(34 nM)
IgG(6.7 nM)
IgG(670 pM)
IgG(67 pM)
(a)
Δf (kHz)
Time (min)
67 nM
34 nM
6.7 nM
670 pM
67 pM
(b)
|Δf| (Hz)
Time (min)

Fig. 5

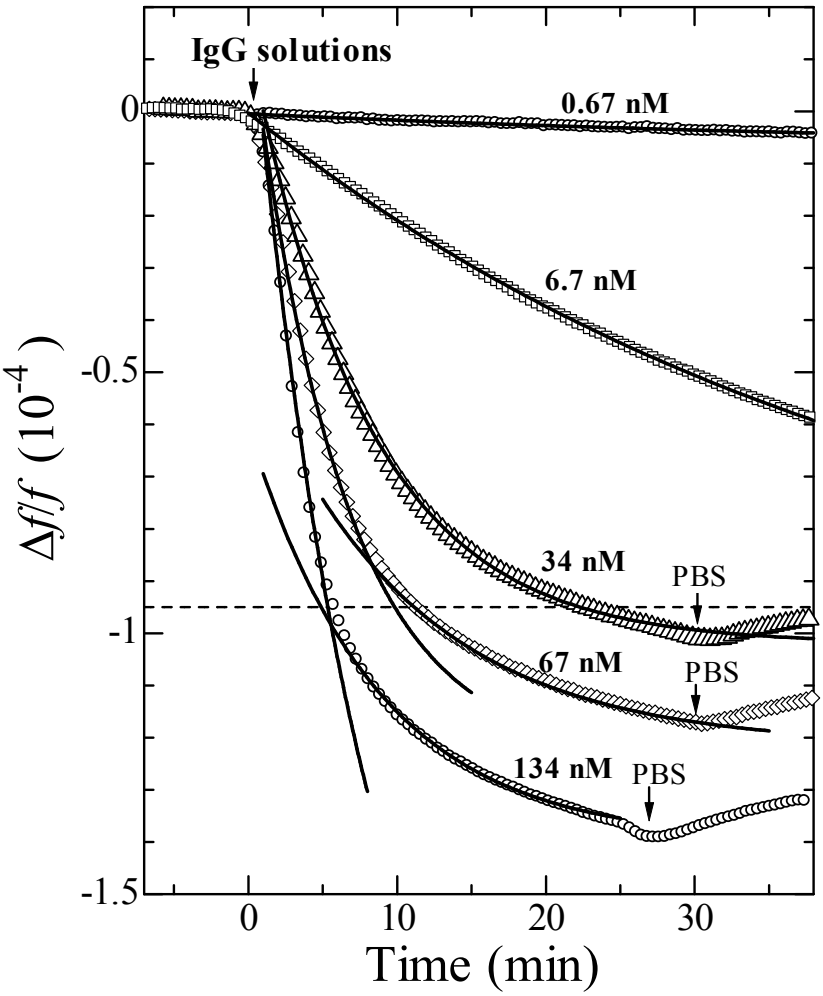
IgG solutions
0.67 nM
6.7 nM
34 nM
PBS
67 nM
PBS
134 nM
PBS
0
-0.5
-1
-1.5
Δf/f (10-4)
0
10
20
30
Time (min)

Fig. 6

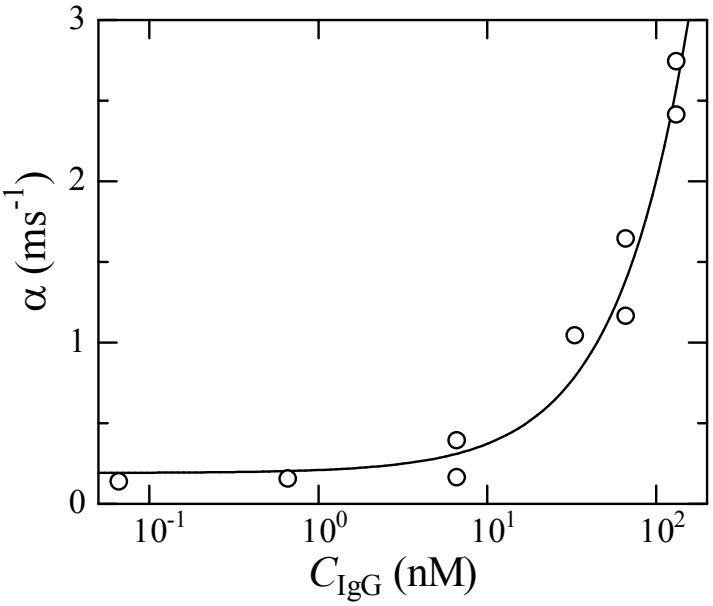

Fig. 7

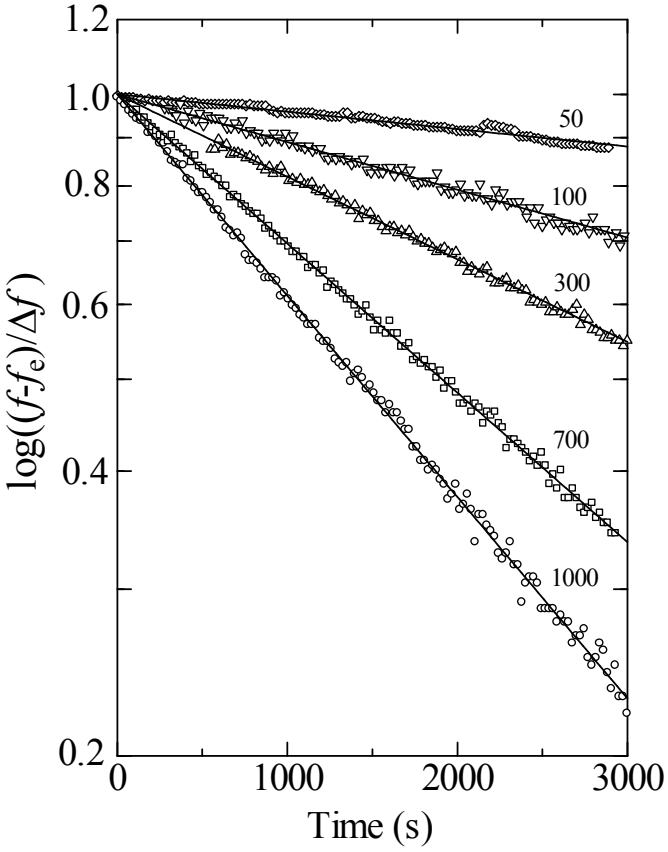
1.2
1.0
0.8
0.6
0.4
0.2
0
1000
2000
3000
Time (s)
log((f-fe)/Δf)
50
100
300
700
1000

Fig. 8

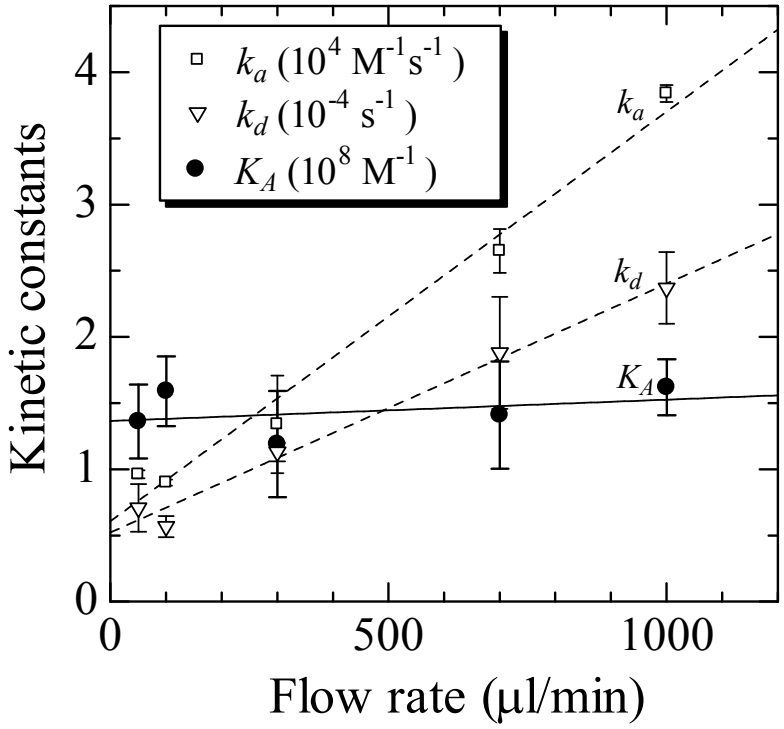
k_a (10^4 $M^{-1}s^{-1}$)
k_d (10^{-4} s^{-1})
K_A (10^8 M^{-1})
k_a
k_d
K_A
Kinetic constants
Flow rate (μl/min)
0
1
2
3
4
0
500
1000

Fig. 9

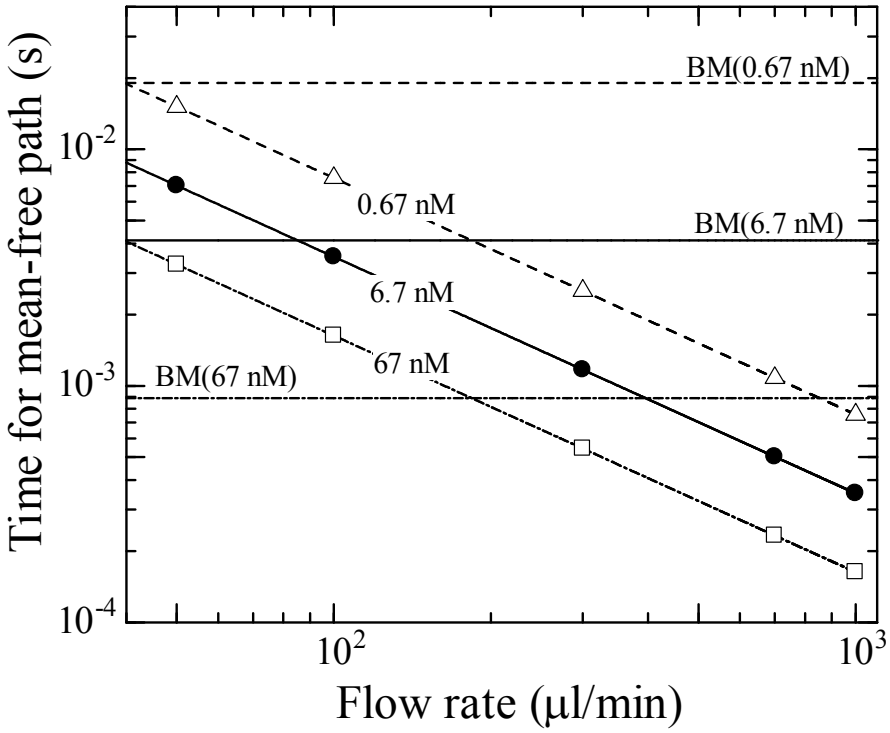
BM(0.67 nM)
0.67 nM
BM(6.7 nM)
6.7 nM
67 nM
BM(67 nM)
Time for mean-free path (s)
10-2
10-3
10-4
102
103
Flow rate (μl/min)

Fig. 10